

## Shortwave feedbacks and El Niño–Southern Oscillation: Forced ocean and coupled ocean-atmosphere experiments

Duane E. Waliser

Institute for Terrestrial and Planetary Atmospheres, State University of New York, Stony Brook

Bruno Blanke<sup>1</sup> and J. David Neelin

Department of Atmospheric Sciences, University of California, Los Angeles

Catherine Gautier

Earth Space Research Group, University of California, Santa Barbara

**Abstract.** Changes in tropical sea surface temperature (SST) can produce changes in cloudiness that modify incoming solar shortwave (SW) radiation, which in turn affects SST. The effects of this negative feedback on Pacific interannual variability are examined in forced ocean model and hybrid coupled ocean-atmosphere model simulations. Two empirical schemes are used to model the large-scale, low-frequency response of surface SW to SST anomalies. The first scheme attempts to account for the nonlocal nature of the atmospheric response to SST based on patterns of covariability analyzed through singular value decomposition. In the observations the primary coupled mode of variability is composed of a SW anomaly in the central Pacific that covaries with anomalous SST in the eastern Pacific. This is applied in the model as a nonlocal SW feedback. The second scheme examines the effects of a purely local feedback with a spatially varying coefficient of magnitude chosen similar to the first scheme. In almost all cases the second scheme behaved similarly to the first, presumably because the correlation scale of SST is large enough for El Niño–Southern Oscillation (ENSO) dynamics that there is little sensitivity to the local approximation in the SW feedback. In simulations forced by time series of observed wind stress the SW feedback induced very minor SST damping. Results from a simplified heat budget analysis showed that while the SW feedback increased the local heat flux damping on SST, it also induced a mean shallowing of the mixed layer. The resulting changes in both the local mean vertical temperature gradient and the zonal velocity response to the wind stress acted to oppose the local heat flux damping effects. When observed SW anomalies were applied to forced simulations, the simulated SST anomalies were modified as expected, and agreement with observed SST improved. In coupled simulations the SW feedbacks had greater impact than in the case of specified stress. The main effects were to decrease the magnitude of the warm and cold SST anomalies in the central Pacific, while leaving the pattern and evolution of ENSO anomalies essentially unchanged elsewhere. The SW feedbacks thus produce a modest improvement of the model ENSO SST pattern compared with observations, although they tended to shorten the period of the model ENSO cycle. Overall the results suggest that large-scale SW feedbacks are of quantitative importance to simulating some aspects of the ENSO cycle but are not critical to the overall occurrence of the phenomenon.

### 1. Introduction

The first models developed to study interannual variability in the tropics were based almost entirely on the wind-driven aspects of the circulation and therefore primarily on ocean dynamics [e.g., Hurlburt *et al.*, 1976; McCreary, 1976]. Although these simplified dynamical models capture some of

the essential characteristics of El Niño–Southern Oscillation (ENSO) events, improving the simulation quality often has involved improving the models' dynamical representation [e.g., Philander, 1981] or internal physical parameterizations (e.g., vertical mixing) [Rosati and Miyakoda, 1988; Blanke and Delecluse, 1993] or implementing more realistic thermodynamic boundary conditions [e.g., Philander, 1981; Rosati and Miyakoda, 1988]. Refining the heat flux boundary conditions can be a particularly challenging problem, the reasons of which stem from the facts that (1) the different character of the four heat flux terms (shortwave, longwave, latent, and sensible) in the surface energy budget makes their separate specification and parameterization difficult and (2)

<sup>1</sup>Now at Laboratoire d'Océanographie Dynamique et de Climatologie, Université Pierre et Marie Curie, Paris, France.

historically, there has been a lack of observations of even moderate quality to examine empirical relationships or to apply to modeling simulations, particularly with respect to the radiative components.

For the tropics the two dominant terms in the surface heat budget are the incoming solar (shortwave) radiation and the outgoing latent heat flux. In most cases the latent heat flux is formulated as a bulk aerodynamic relationship, with a dependence on the sea surface temperature (SST), surface wind speed, sea level pressure, exchange coefficient ( $C_E$ ), and specific humidity of the atmospheric boundary layer. These quantities are provided explicitly, or can be more readily parameterized, in fully coupled simulations by the atmospheric general circulation model (GCM). For forced or hybrid coupled model (HCM) [Neelin, 1990] simulations, the latter three quantities are always parameterized or estimated from observations. There have been many efforts to improve model parameterizations of latent heat flux, [e.g., Philander and Seigel, 1985; Seager et al., 1988; Giese and Cayan, 1993], while efforts for improving surface shortwave (SW) parameterizations have been rare, particularly in the case of including active feedbacks due to atmospheric cloudiness [Harrison, 1991; Gent and Tribbia, 1993].

In an analysis of interannual variability in SST and satellite-derived SW, Chertock et al. [1991] showed that the 1982 ENSO warming in the eastern Pacific preceded a sharp drop in the net surface SW, which then preceded a mild cooling of the SST. In an analysis of radiation products derived from the Earth Radiation Budget Experiment (ERBE), Ramanathan and Collins [1991] hypothesized that because of the observed super greenhouse effect in the deep tropics, a cirrus-cloud thermostat mechanism acts to regulate SST warming. These studies, in combination with studies of the relationship between deep convection and SST [e.g., Graham and Barnett, 1987; Waliser and Graham, 1993], suggest a possible negative feedback mechanism due to SST-forced cloudiness that may be operating to damp out the extreme phases of the ENSO cycle. This mechanism, which would act to diminish SST warming/cooling in the central Pacific, has not been explicitly addressed in modeling studies of ENSO variability. Moreover, there has been a tension between studies that postulate a major role for SW feedbacks and models that do not include SW feedbacks but yet simulate plausible ENSO cycles [e.g., Zebiak and Cane, 1987; Battisti, 1988; Philander et al., 1992]. It is our purpose to address this question quantitatively.

In this paper we develop two simple empirical models of the negative feedback mechanism associated with large-scale, low-frequency SST-forced cloudiness, and we apply them to coupled and forced ocean simulations of interannual variability. The first model is based on singular value decomposition [see Bretherton et al., 1992] of SST and SW anomalies over the tropical Pacific. This model attempts to capture the instantaneous, field-to-field relationship between the SST and SW anomalies, and thus potentially any remotely forced coupling between these variables. The second SW model is based on the local SST anomaly only and has a spatially varying feedback amplitude. The point of applying this local scheme is to determine whether SST changes in the eastern Pacific are important in the character of the SW feedback, which is primarily localized in the central Pacific. In addition to applying these simplified SW feedback schemes we also apply observed shortwave anomalies be-

tween July 1984 and December 1989 to a forced run to evaluate their impact on the simulation of the tropical Pacific. In the following section the data sets used in this study are described. In section 3 the empirical SW feedback schemes are developed. In section 4 the ocean model and experimental setup are described. In sections 5 and 6 the results of the forced and coupled ocean model experiments are presented. Section 7 concludes with a brief summary and discussion.

## 2. Data

The observation data sets used in this study are gridded values of SST, net surface shortwave, highly reflective cloud (HRC), outgoing longwave radiation (OLR), pseudo wind stress, and climatological heat flux data.

The SST data set is constructed from an in situ measurement analysis from 1971 through 1981 joined with a blended analysis of satellite-derived and in situ measurements from 1982 through 1990, each provided monthly, on a global,  $2^\circ \times 2^\circ$  grid [Reynolds, 1987]. The net surface shortwave is a satellite-derived product developed by using the method of Gautier et al. [1980], using the International Satellite Cloud Climatology Project (ISCCP) Stage C2 data products [Rossow and Schiffer, 1991]. The SW data are provided monthly on a global,  $2.5^\circ \times 2.5^\circ$  grid, from July 1984 to December 1990 [Wang, 1994]. These data sets are used in the development of the empirical schemes that obtain shortwave anomalies from SST anomalies and, in the case of SST, for validation of forced model simulations.

OLR is an estimate of the total outgoing infrared (IR) radiation at the top of the atmosphere inferred from multi-band satellite radiation measurements [Gruber and Krueger, 1984]. It has been used in many studies as an indicator of cloudiness over the tropical oceans, particularly deep convective systems [e.g., Liebmann and Hartmann, 1982; Rasmusson and Wallace, 1983; Graham and Barnett, 1987]. The OLR data set used in this study was constructed by Horel and Cornejo-Garrido [1986] from daytime and nighttime archived OLR estimations (in watts per square meter), interpolated onto a  $2^\circ \times 2^\circ$  grid between  $30^\circ\text{N}$  and  $30^\circ\text{S}$  for the global tropics, and then time-averaged into 5-day means; these were subsequently averaged in monthly values. The data set extends from June 1974 to May 1988 with gaps of 10 months during 1978 and 2 months during 1987.

HRC [Garcia, 1985] is a daily, binary indicator of the presence of organized deep convection based on the subjective analysis of visible and IR satellite mosaics (daytime only). The IR data are used as a proxy for cloud top height and thus to indicate the presence of high clouds, specifically convective systems. The visible information is used to exclude the large-scale cirrus clouds associated with convective systems. The results from this analysis are combined in the form of binary-valued, daily "images" with  $1^\circ$  spatial resolution that indicate regions where large-scale convection is present. These daily images are combined to form monthly values, e.g., days per month deep convection was present at each grid point, from 1971 through 1987.

The OLR and HRC have been compared with the ISCCP stage C2 cloud products by Waliser et al. [1993]. When used as proxies for deep convection, both products compared favorably with the ISCCP C2 convective index, particularly in the convergence zones. In addition, the OLR correlates

fairly well with total high and total mid-level cloud amount. These two convective/cloud-related products are used to extend the SW data set backward to 1971 in order to provide more confidence in the representation of the principal coupled SST-SW mode. It should be noted that SW variability due to low clouds is not well represented by either the OLR or HRC.

For the development of the empirical SW feedback schemes, all the above data sets were mapped to the same  $4^\circ \times 8^\circ$  (latitude  $\times$  longitude) tropical Pacific domain grid. This coarse grid was required in order to perform the singular value decomposition (SVD) and canonical correlation (CC) analyses using modest computational resources. In addition, the SW was also mapped to the same  $2^\circ$  grid as the original SST in order to analyze some aspects of the local relationship between SW and SST.

The pseudo wind stress is a product constructed at Florida State University [Legler and O'Brien, 1984]. The actual wind stress is obtained by multiplying the pseudo wind stress times a drag coefficient ( $C_d$ ). The resulting wind stress is used (1) to force the ocean model in the uncoupled simulations, (2) to produce the mean state of the ocean model used in the coupled simulations, and (3) in the formulation of the statistical atmosphere for the coupled simulations (see section 4 for more details). The heat flux boundary conditions for both the coupled and uncoupled simulations are derived from the long-term annual mean and annual cycle net heat flux data of Oberhuber [1988]. This actual specification of the heat flux boundary conditions is described in more detail in section 4.

### 3. Observational Analysis and Empirical Models

The monthly SW and SST data were used as inputs to SVD and canonical correlation analysis (CCA) to construct an anomaly model for SW. The SVD and CCA techniques are described by and compared with other approaches for extracting modes of covariability between two data sets Bretherton et al. [1992]. Various approaches, including SVD and CCA, for analyzing or constructing empirical components of atmospheric forcing based on SST patterns have been used by Graham et al. [1987] (CCA), (SVD), Barnett et al. [1993], H.-H. Syu et al. (Seasonal and interannual variability in a hybrid coupled GCM, submitted to *Journal of Climate*, 1994) (hereinafter referred to as SNG, 1994), and others to derive the wind stress anomaly fields from the SST field. The intent here is to use these techniques to capture the dominant interannual mode(s) of covariability between SST and SW. Although the SVD and CCA techniques have comparable properties, both were applied to the data to ensure the characteristics of the primary modes extracted were not dependent on the particular method.

Figure 1 shows the spatial patterns and time series of the first interannual mode of covariability between SW and SST, extracted via SVD analysis. For the mode shown, the annual cycle has been removed from the data before the decomposition. The mode shown in Figure 1 accounts for 89% of the covariability in the combined anomaly fields, 45% of the SST variability, and 18% of the SW variability. Figure 1a shows the SST anomaly pattern, which is dominated by the strong warming/cooling signature in the eastern and central Pacific that is associated with the ENSO phenomena [e.g., Rasmus-

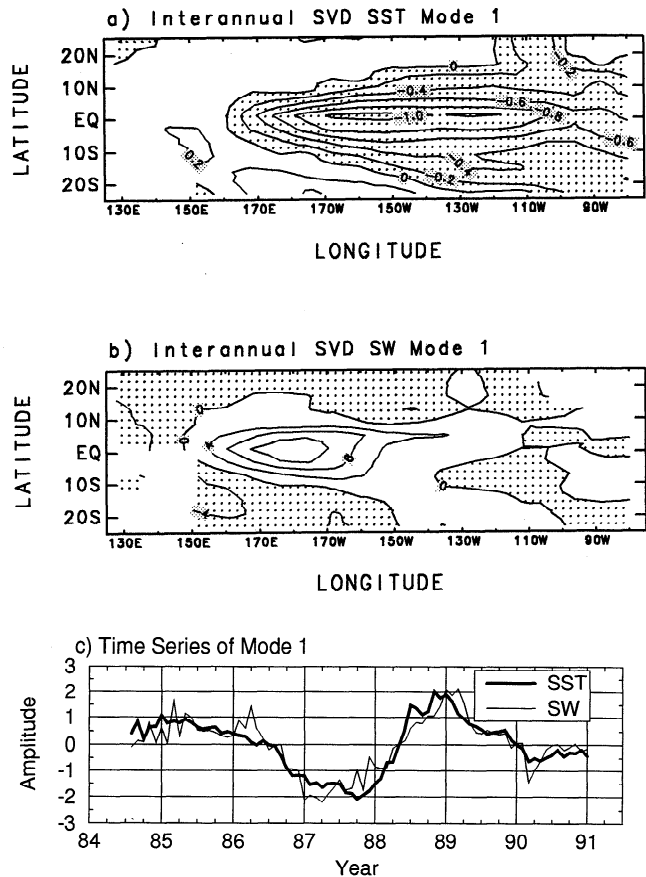


**Figure 1.** First empirical, interannual, coupled (a) SST and (b) SW mode extracted using SVD decomposition from data between July 1994 and December 1990 and (c) time series coefficients of SST (thick line) and SW (thin line) modes. SST and SW time series are normalized by the variance of the associated fields shown in Figures 1a and 1b, respectively.

son and Wallace, 1983; Cane, 1983]. The maximum pattern value occurs along the equator between about  $170^\circ\text{W}$  and  $120^\circ\text{W}$  and has a magnitude of about  $1^\circ\text{C}$ . Figure 1b shows the corresponding anomaly pattern in SW. Here the maximum response is near the dateline and has a magnitude of about  $14 \text{ W m}^{-2}$ . Figure 1c shows the corresponding normalized time series for the projections of observed SST and SW onto this mode's spatial patterns.

As is evident from Figure 1, a strong positive SST anomaly in the central and eastern Pacific, such as in 1986–1987, is associated with a negative SW anomaly in the central Pacific. This negative SW anomaly is due to the eastward movement of convection into the central Pacific region of ocean warming. While it is still a subject of some debate why the SW anomaly is centered near the dateline, even though the maximum response in SST is to the east, it presumably is associated with the total SST being too low in the eastern Pacific, relative to other regions, to support deep convection—the likely source of much of the cloudiness. This cloudiness blocks a significant amount of solar radiation and produces negative anomalies in the region of the dateline of about  $-30 \text{ W m}^{-2}$ . Maximum monthly anomalies on the original  $2.5^\circ$  data grid are between about  $+30 \text{ W m}^{-2}$  and  $-60 \text{ W m}^{-2}$ .

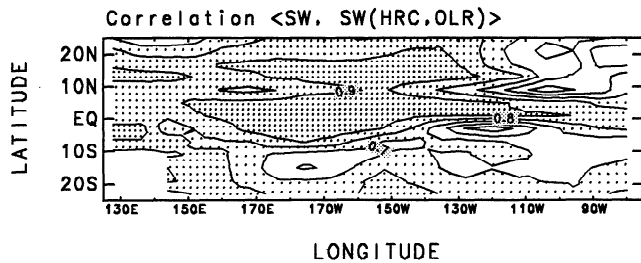


**Figure 2.** Correlation coefficient between satellite-observed net surface SW anomalies (about the annual cycle) and the SW anomalies derived from the HRC and OLR using a CCA-based model. Time period is between July 1984 and December 1987 (see section 3 for details).

In order to provide an increased level of confidence in the above spatial patterns of SST and SW, two additional analysis procedures were performed. First, the same modal analysis was performed by using CCA, which extracts modes of covariability with maximum correlation in time (in this case). In contrast, SVD extracts modes of covariability with maximum covariance. The CCA analysis produced patterns of spatial variability and time series very similar to those shown for SVD in Figure 1. The principal difference was that the temporal coefficients for the CCA modes were slightly better correlated, as would be expected. For the purposes of this study the differences are negligible, and the SVD mode shown in Figure 1 was applied.

In the second analysis, HRC and OLR data were used to extend the SW series backward. Since the analysis period shown in Figure 1 encompasses only one ENSO “cycle,” it was desirable to extend the SW backward in order to redo the analysis over a time period encompassing more ENSO events. In this analysis, overlapping months of HRC and OLR with SW (July 1984 to December 1987, 42 months) were used to construct a CCA-based anomaly model [e.g., *Graham et al.*, 1987] of SW based on the HRC and OLR combined fields. The first 12 modes from the CCA analysis were used to construct SW anomalies from HRC and OLR anomalies. The success of the HRC-OLR SW model in reconstructing the 42 months of SW data is indicated in Figure 2, which shows the correlation between the satellite-observed SW and SW constructed via the CCA model using HRC and OLR. The model data were smoothed in time using a 3-point box filter and smoothed in space using a 5-point cross filter prior to computing the correlation. The three stippling densities in the figure show areas of correlation greater than 0.7, 0.8, and 0.9. In most areas of the tropical Pacific the derived shortwave agrees fairly well with the satellite values. However, there are areas of poor agreement, such as the eastern Pacific, particularly south of the equator and near the Intertropical Convergence Zone (ITCZ). It is most likely that SW variability due to low clouds—which the HRC attempts to filter out and which the OLR is less sensitive to [*Waliser et al.*, 1993]—is contributing to much of the disagreement in these regions. The CCA was also performed with the HRC and OLR data sets separately. The results indicated that the HRC enhanced predictability in the near-equatorial, central Pacific, while the OLR added predictability in regions away from the equator.

Figure 3 is analogous to Figure 1, except that it shows the

SVD results for the SST and SW series extending from 1971 to 1990. In this case the SW between January 1971 and May 1974 was derived from the HRC, and that between June 1974 and June 1984 from the HRC + OLR. This mode accounts for 93% of the covariability in the combined anomaly fields, 45% of the SST variability and 28% of the SW variability. The spatial patterns of SST and SW (Figures 3a and 3b) are very similar to those in Figure 1. The temporal evolution of the two patterns shows strong warming events in 1972–1973, 1982–1983, and 1986–1987, with modest events in 1977, 1980, and 1990. The analysis just described, along with the corresponding results in Figures 2 and 3, are presented to show that while the mode of covariability shown in Figure 1 was obtained from only 6.5 years of data and only one ENSO event, there is reason to believe that it is a fairly good characterization of the spatial relationship between large-scale interannual SST and SW anomalies in the tropical Pacific.

The presentation above regarding the results of the SVD analysis, along with the intent to use it to predict SW anomalies from SST anomalies, makes three major assumptions. The first is that large-scale anomalous SW is linearly related to large-scale anomalous SST. Figure 4 shows a scatterplot of the SST and SW projection coefficients from Figure 1c, multiplied by the square root of the variance of their corresponding SVD pattern (Figures 1a and 1b). The plot shows that these field-to-field SST and SW coefficients,

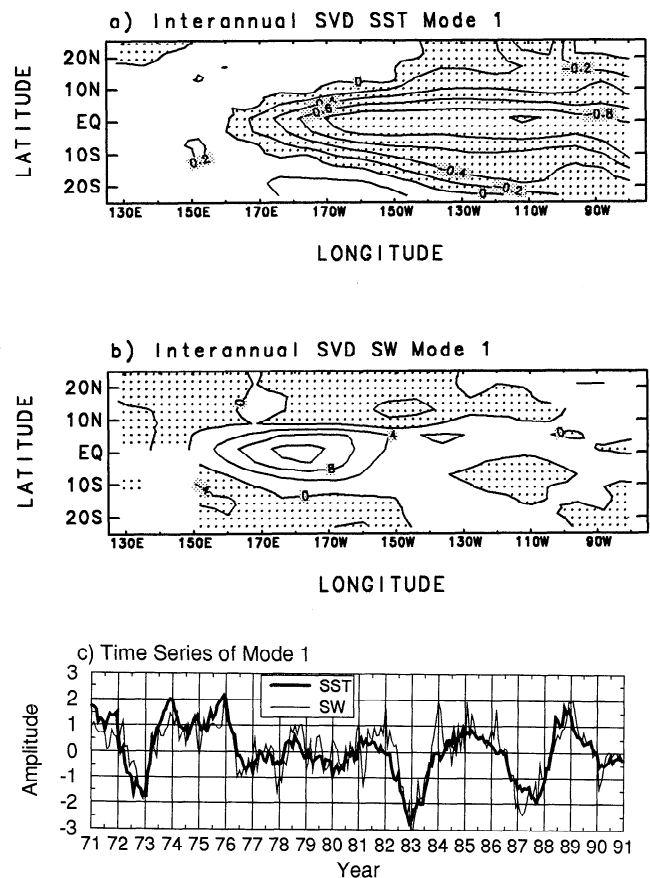


**Figure 3.** As in Figure 1, except from an extended SW data set produced from the CCA-based model using HRC and OLR. In this case the SST and SW data sets extend from January 1971 through December 1990.

to a good approximation, are linearly related, with a linear correlation coefficient of 0.89. Thus for the single SW–SST mode investigated here, which indicates a coupling between the SW anomalies in the central Pacific to the SST anomalies in the central/eastern Pacific, the linear approximation is reasonable.

The second assumption required to make use of this relation as a model for SW feedbacks is that the SW variations are caused by the SST variations. Support for this assumption is based on a priori knowledge of tropical atmospheric dynamics and on the conformity between expectations based on this and the empirical results. The tropical atmosphere is expected to be substantially in adjustment with forcing by lower boundary conditions on time scales longer than a month, certainly on the long time scales that dominate in Figures 1c and 3c. Furthermore, the short-wave pattern corresponds well to the shifting of the convergence zone associated with ENSO SST warming, both as observed and as reproduced in GCM experiments with specified SST variations [e.g., Lau, 1985].

The third assumption implicitly made in the construction of the SVD-based SW feedback is that it is necessary to examine the covariability of the entire spatial fields of SST and SW in order to obtain the proper large-scale SW response to a given SST anomaly pattern. Figure 5 shows scatterplot density diagrams of SW versus SST anomalies (about the annual cycle) from  $2^\circ \times 2^\circ$  gridded data from four different regions of the tropical Pacific: western Pacific (Figure 5a), central Pacific (Figure 5b), eastern Pacific ITCZ (Figure 5c), and southeastern Pacific (Figure 5d). The diagrams illustrate that the local relationship between SST and SW is rather weak except in the central Pacific region, and even in this region it includes a significant amount of noise. The more apparent linear relation exhibited by the central Pacific probably stems from the equilibrium SST of the region being in an SST range of about  $26^\circ\text{--}28^\circ\text{C}$ , where deep convection is generally most sensitive to changes in SST [e.g., Graham and Barnett, 1987].

Given the results in Figures 1, 4 and 5, and those from several studies that examine the relationship between convection and SST [e.g., Gadgil et al., 1984; Neelin and Held, 1987; Graham and Barnett, 1987; Waliser and Graham, 1993], it is plausible that the response in SW, shown in Figure 1b, occurs only in, and near, the central Pacific because the anomaly warming in this region is able to raise the total SST to a level that can better support the organization of large-scale convection. In this context the near-equatorial regions in the eastern Pacific would show a negligible SW response because the total SST is still generally less than  $26^\circ\text{C}$ , a value usually observed to be too low to support deep convection. This raises the questions of how big a role SST warming in the eastern Pacific plays in the development of the shortwave feedback that is localized in the central Pacific, and how this role affects the evolution of the modeled interannual variability.

To address this question of local versus remote SW forcing by SST, we have developed a second SW feedback that is based on the local SST anomaly only. This scheme consists of a spatially varying heat flux damping coefficient, of maximum amplitude of  $-20 \text{ W m}^{-2} \text{ K}^{-1}$ , multiplied by the local SST anomaly. The spatial distribution of the damping coefficient is shown in Figure 6. This pattern was based on the relationships between SW and SST anomalies

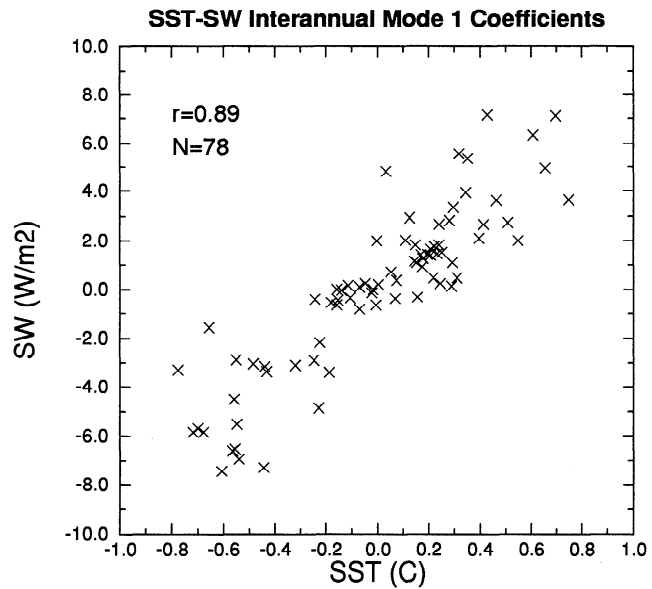


**Figure 4.** Scatter diagram of mode 1 SST and SW projection coefficients from Figure 1c. To obtain dimensions, the coefficients were multiplied by the square root of the variance of the corresponding spatial pattern (e.g., Figures 1a and 1b).

shown in Figure 5 and on the SW response pattern shown in Figure 1b. The maximum value of  $-20 \text{ W m}^{-2} \text{ K}^{-1}$  is consistent with earlier observational analyses [e.g., Chertock et al., 1991; Ramanathan and Collins, 1991] and with values obtained from linear regression of SW and SST anomalies from the central Pacific. This feedback affects approximately the same region of the Pacific as the nonlocal feedback (Figure 1b), but it is dependent only on the local SST anomaly, rather than on a weighted distribution of entire SST anomaly field (Figure 1a). We note that at the small scales at which this feedback is being applied (i.e., model grid), the atmospheric response to SST could never be truly local. However, the two feedback schemes examined here provide useful limits for investigating SST-induced SW feedbacks. In the local case the spatial correlation of SW is due entirely to the autocorrelation scales of the SST, while the SVD SW feedback likely exaggerates the nonlocality of the relationship due to the enhanced autocorrelation of SST along the equator associated with ocean dynamics. It is likely that reality lies somewhere between these two limits.

#### 4. Model Description

The ocean model used for the numerical simulations presented is the Geophysical Fluid Dynamics Laboratory (GFDL) modular ocean model (MOM) based on that of Cox [1984]. The active model domain extends between  $130^\circ\text{E}$  to  $80^\circ\text{W}$  and  $30^\circ\text{S}$  to  $50^\circ\text{N}$ . The model contains realistic continental boundaries with a flat ocean bottom. Between  $10^\circ\text{S}$  and  $10^\circ\text{N}$  the grid spacing in latitude is  $0.5^\circ$ , with grid spacing increasing poleward to about  $4^\circ$  near the boundaries. The grid spacing in longitude is  $1^\circ$  near the western boundary and increases to  $3^\circ$  in the central and eastern part of the basin. The model has 27 vertical levels, 10 of which are in the upper 100 m. Vertical mixing coefficients are functions of the local

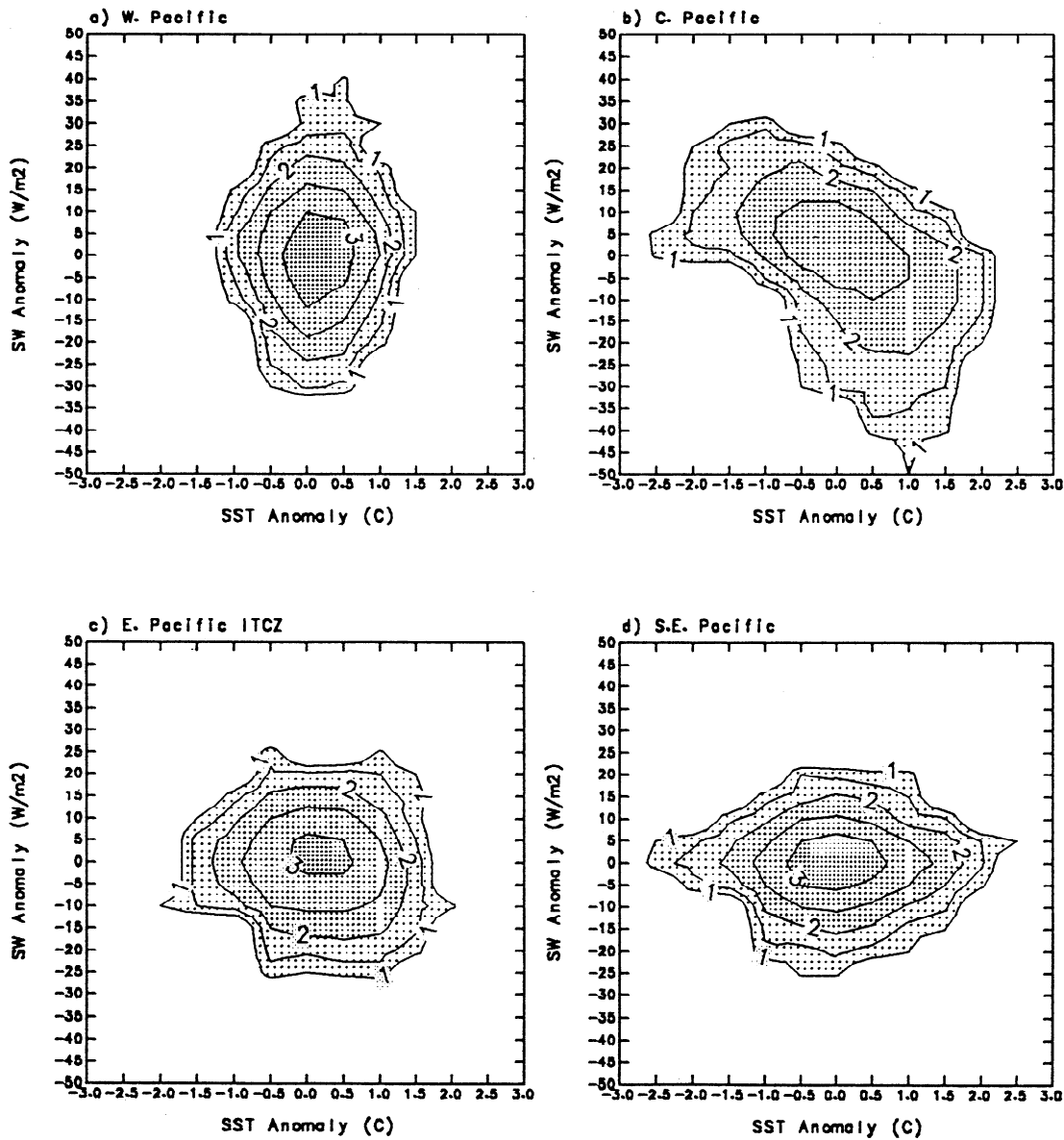


**Figure 5.** Scatter diagrams of SST anomalies against net surface shortwave anomalies from the (a) western Pacific, (b) central Pacific, (c) eastern Pacific ITCZ, and (d) southeastern Pacific. Anomalies are taken about the annual cycle.

Richardson number, similar to those derived by *Peters et al.* [1988] from in situ measurements. Shortwave penetration into the mixed layer is taken into account by using a formulation based on the measurements of *Paulson and Simpson* [1977].

The ocean model is run in both a forced and a coupled configuration. In the standard configuration of the forced simulations the surface boundary conditions are specified as follows: (1) the monthly varying wind stress forcing is calculated from the Florida State University (FSU) pseudo-wind-stress product with a constant drag coefficient of  $1.2 \times 10^{-3}$ ; (2) the freshwater flux is modeled as a relaxation of the surface salinity to climatology [*Levitus*, 1982]; and (3) the heat flux boundary condition is composed of the observed annual cycle of net heat flux [*Oberhuber*, 1988] with an added negative feedback term [*Syu et al.*, 1993]. This negative feedback is based on the derivative of the heat flux

formulation of *Seager et al.* [1988] with SST, which gives the following:

$$dQ/dSST = -\rho L C_E U (1 - \delta) dq_s/dSST + \alpha$$

where  $\rho$  is the surface air density,  $L$  is the latent heat of vaporization,  $U$  is the mean wind speed,  $C_E$  is the bulk exchange coefficient, and  $\alpha$  is a constant equal to 1.5,  $\delta$  is the ratio of the specific humidity of boundary layer air ( $q_a$ ) and the saturation specific humidity at the SST [ $q_s(SST)$ ] and is fixed at a constant value equal to 0.75. As applied here, the feedback varies in space and is constant in time and is calculated from observed values of the long-term mean wind speed and SST [*Oberhuber*, 1988]. The values range from about  $-17 \text{ W m}^{-2}$  to  $-30 \text{ W m}^{-2}$  over the tropical Pacific domain. With this formulation the model does not contain any active evaporation-wind feedback (i.e., due to wind anomalies) in the simulations presented.

In the standard configuration of the coupled simulations the atmospheric component providing the surface wind stress is an empirical model based on the linear relationship between wind stress anomaly patterns and SST anomaly patterns computed by using SVD. In order to produce interannual variability with an amplitude consistent with observations, the surface wind stress anomalies computed by the SVD-wind model are multiplied by an additional “coupling coefficient” of 1.2. These aspects of the HCM are described by SNG (1994). The mean stress is obtained from the FSU pseudo wind stress, using a drag coefficient of  $1.2 \times 10^{-3}$ . The surface heat flux is given as described above but using long-term annual mean flux instead of seasonally varying quantities. Thus the HCM simulations here do not contain, or simulate, an annual cycle and are designed to examine only the interannual oscillations within the coupled system. The choice of conducting the coupled experiments in the absence of the annual cycle was made after careful consideration. The main advantages are that (1) it provides the simplest, cleanest case in which to analyze the impacts of the target mechanism, (2) the effect on the inherent ENSO period may be seen, and (3) we know that the basic spatial pattern and ENSO mechanisms are the same in this model when the annual cycle is included but frequency locking occurs.

## 5. Forced Model Simulations

The forced model simulations are 12-year integrations, from 1978 to 1989. They begin from an “equilibrium” state that was achieved by forcing the model with long-term mean wind stress and heat flux (as described above) for 3 years, followed by forcing the model with mean annual cycle wind stress and heat flux for 3 more years. Due to the long time scales associated with the deep ocean circulation, this state constitutes an equilibrium adjustment only in the upper layers of the ocean, primarily those lying above the thermocline. The simulation forced with the standard model physics and no SW feedback is denoted Standard. In the two SW feedback cases the added SW anomaly due to the feedback scheme is computed once each simulated day. For the SVD-SW case, this requires projecting the SST mode shown in Figure 1a onto the model SST anomaly, normalizing by the variance of the mode, multiplying the resultant coefficient by the SW mode (Figure 1b), and then adding this to the total heat flux. For the local SW case the feedback is computed by multiplying the model SST anomaly by the local negative feedback coefficient (Figure 6) point by point and adding this to the total heat flux.

Figures 7a and 7b show time-longitude plots of the interannual, equatorial SST anomalies averaged between  $1^{\circ}\text{N}$  and  $1^{\circ}\text{S}$  for the Standard simulation and from observations, respectively. Figure 7c shows the difference between Figures 7a and 7b and thus indicates how well the standard model physics simulates observed SST anomalies in the equatorial Pacific. Overall the agreement is quite good; however, the simulated warm events for both the 1982 and 1986 ENSOs extend further to the west and are slightly warmer than the observations. Likewise, the simulated cold event in 1984 also extends further to the west and is slightly cooler. In the eastern Pacific the differences between the observations and simulation are more pervasive. The cool events occurring in 1981 and 1985 in this region are stronger

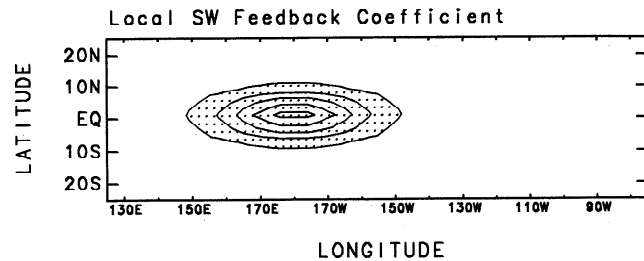


**Figure 6.** Amplitude of the heat flux negative feedback representing the local SW feedback scheme. Contours are  $4 \text{ W m}^{-2} \text{ K}^{-1}$ , unshaded regions have amplitude near zero, and the maximum value is  $-20 \text{ W m}^{-2} \text{ K}^{-1}$ . SW feedback is computed by multiplying the local SST anomaly by the local heat flux negative feedback value.

in the model than in the observations, while the warm event occurring in 1987 is weaker. Moreover, in the eastern Pacific there are spurious anomalies in late 1985 (warm) and late 1989 (cold) that are not found in the observations.

By adding either of the negative feedbacks discussed in section 3 we might expect the excessive excursions of anomalous SST into the western central Pacific in the Standard simulation discussed above to be reduced. Further, we would expect little impact on the SST in the eastern Pacific. Figure 8a shows a time-longitude diagram analogous to that in Figure 7c, except for the difference between the observations and the forced simulation that includes the SVD-SW feedback. The figure shows that generally the impact of the feedback is rather small, with the principle effects being (1) the 1982–1983 warm anomaly begins further west, extends in a more continuous fashion across the basin to the eastern Pacific where its magnitude is slightly larger, and decays slightly faster near the dateline and (2) the excessive warming produced by the simulations near the dateline during the 1986–1987 ENSO is slightly greater. Figure 8b shows the same result as Figure 8a, except for the local SW feedback. This figure shows that the local SW feedback has nearly the same impact on the simulation as the SVD feedback, with only a slightly greater damping effect during the central Pacific warm events.

Figure 9 shows the amplitude of the SST-SW feedback—the projection of the SST mode (Figure 1a) onto the model SST anomaly—that was calculated during forced SVD-SW simulations (thick solid line). Also shown are the projection of the SST mode onto the observations during 1978–1989 (thick gray line) and onto the Standard simulation (thick dashed line). The comparison of the forced model curves with the observations gives another indication of how well the model simulates the observed ENSO variability, and it highlights the minor impact made by the SW feedback. Comparing the Standard forced case with the observations shows that the 1982–1983 ENSO event is fairly well simulated, with only modest discrepancies in the magnitude and phase of the warm episode. However, the plot also shows that the simulation of the 1986–1987 ENSO event was not as good in terms of its evolution or magnitude. The observed event contains one long-lasting episode with a fairly smooth evolution. The simulated event shows a sequence of two shorter-lived warmings with more modest amplitudes. Inspection of the forced SVD-SW case shows that this characteristic is still apparent, with many of the small peaks and

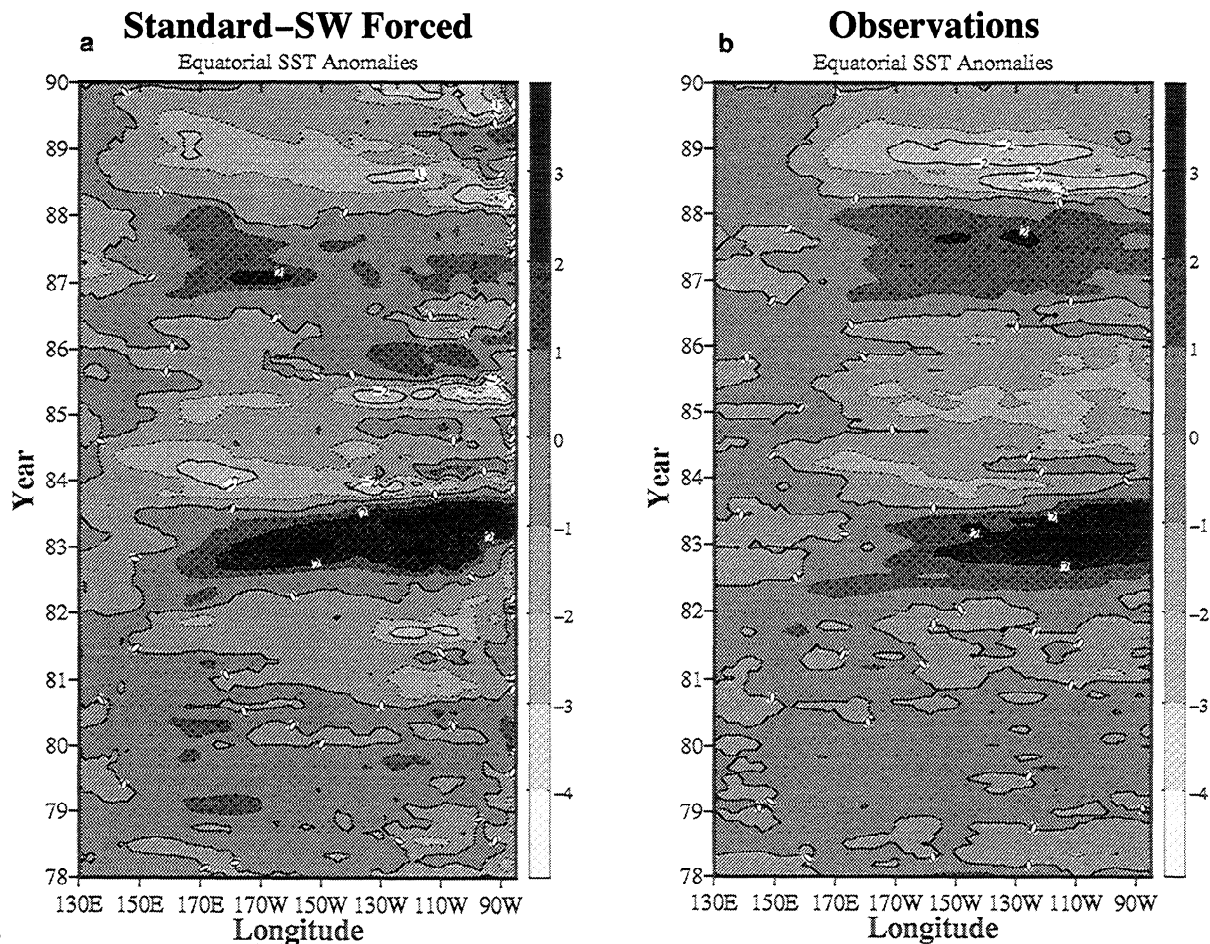


**Figure 7.** Time-longitude diagram of the interannual SST anomalies on the equator from (a) the Standard simulation and (b) observations and (c) time-longitude diagram of the difference between the SST anomalies on the equator from Standard simulation and the observations. Equatorial sections are averaged between 1°N and 1°S.

valleys slightly accentuated over those in the Standard simulation. While the smallness of the SST damping produced by the SW feedback was somewhat unexpected, the occurrence of accentuated anomalies was certainly unexpected.

In order to illustrate why the SW feedback simulations did not exhibit the expected behavior it is instructive to analyze the evolution of the SST in the region near the dateline where the feedback due to the SW flux is greatest. This analysis, presented in detail in the appendix, indicates that the SW feedbacks, as applied here, induce changes in the model mixed-layer dynamics that offset and often outweigh the more obvious effects of a simple increase in the local heat flux damping. The added SW surface heat flux damping not only increases the local (explicit) negative feedback on SST but also induces a mean shallowing of the mixed layer. Figure 10 shows time-longitude diagrams of equatorial mixed-layer depth averaged between 0.5°N and 0.5°S for the Standard and SVD-SW simulations. The mixed-layer depth was computed as the depth where the subsurface temperature is 1°C less than the SST. The effect of the SW feedback is to reduce the mixed-layer depth, primarily in the central and western Pacific, by about 10–40 m, with an average reduction near the dateline of about 20 m. Each of these

effects, increased local heat flux damping and reduced mixed-layer depth, promotes a local decrease in the amplitude of the SST anomaly. However, due to the shallower mixed layer, the mean vertical temperature gradient and the zonal velocity response for a given wind stress are larger, each of which leads to a local increase in the amplitude of the SST anomaly. In the cases of the forced simulations presented here, these opposing effects tend to balance such that the SST anomaly amplitude is essentially the same for the Standard and SW feedback cases.

In light of the above results it is of interest to investigate the effects of applying the observed SW anomalies, i.e., without including the feedback from the SST. Figure 11a shows a time-longitude diagram at the equator, averaged between 1°N and 1°S, of the observed SW anomalies. The SW anomalies are unavailable before July 1984. Note that the largest shortwave anomalies occur in the central Pacific during the warm phase of the 1986–1987 ENSO, in which there is about a  $40 \text{ W m}^{-2}$  reduction in SW, and during the subsequent La Niña event in 1989, in which there is about a  $20 \text{ W m}^{-2}$  increase in SW. Figure 11b shows an analogous time-longitude diagram of the difference between the SST from the simulation forced with these SW anomalies and the observed SST. The simulated SST field shows that the

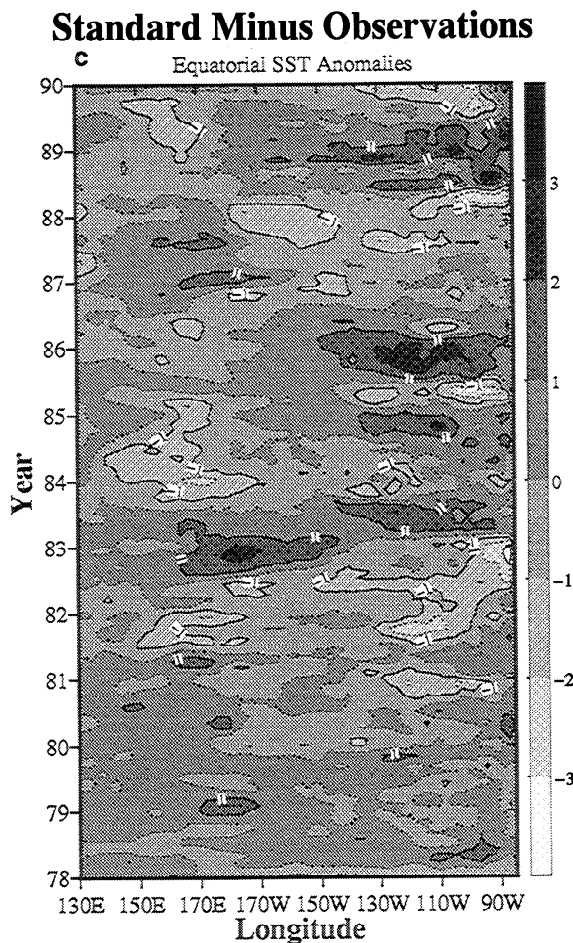


Figure 7. (continued)

observed shortwave induced a stronger impact on the system than either of the parameterizations and provided for better agreement between simulation and observations in the western and central Pacific (compare with Figure 8). Figure 11c shows the difference in the Standard simulation and the simulation with observed SW anomalies and thus gives a more clear indication of the impact of the “observed” SW. Each of the two large-scale SW anomalies acts to damp out the associated warm and cold events, by about  $-0.8^{\circ}\text{C}$  and  $+0.4^{\circ}\text{C}$ , respectively.

It is worth mentioning that a simulation was performed in which only the first SVD mode of the observed SW anomalies (i.e., Figures 1b and 1c) was applied. The results from this “filtered” SW simulation (not shown) and the simulation using the unfiltered SW (described above) were nearly the same along the equator. However, in the far western Pacific, where modeled SST has been shown to be particularly sensitive to small changes in applied heat flux [e.g., Harrison, 1991], and in regions away from the equator, the filtered SW simulation had poorer correlation between observed and modeled SST. This latter difference is expected, since the filtered SW contains essentially no SW information in the off-equatorial regions. However, the nearly identical behavior of equatorial SST in these two simulations indicates that modeling the observed SW feedbacks related to ENSO variability can be based primarily on the large-scale features of the near-equatorial SW field, most notably the variability

located in the central Pacific. It is also worth noting that the correlation of model SST with observations in off-equatorial tropical regions (not shown) is only slightly better in the case with observed SW specified than in other cases. This suggests that, at least in the near term, the amount of improvement in simulation and prediction of off-equatorial tropical SST that can be obtained by including cloudiness may be modest.

## 6. Coupled Model Simulations

Three coupled simulations were performed to determine the role SST-forced SW variability may play as a negative feedback in the evolution of ENSO. Each of the coupled model simulations begins from a reference state with an added wind stress impulse, and is then integrated for 12 years. The reference state was achieved by forcing the ocean model with the heat flux formulation described in section 4 and long-term annual mean wind stress for 3 years, consistent with a state of upper ocean “equilibrium” (as discussed earlier). This state is in fairly good agreement with the observed long-term annual mean conditions of the tropical Pacific, the two of which are shown in Figure 12. The first case, referred to as the Standard, is composed of the standard model physics and boundary conditions with wind stress feedbacks described in section 4; it does not include any negative feedbacks due to shortwave. The second case includes the coupling of the SVD-SW feedback, while the third case includes the coupling of the local SW feedback.

Figure 13 shows time-longitude diagrams of SST anomalies about the 12-year mean along the equator, averaged between  $1^{\circ}\text{N}$  and  $1^{\circ}\text{S}$ , for the coupled simulations. In the Standard case (Figure 13a) the oscillating warm and cold events have a dominant period of about 29 months. The model ENSO events are similar to those described by SNG (1994) (for the case without the seasonal cycle), although the period differs due to the different vertical mixing parameterization used here. The variability is characterized primarily as a standing oscillation in SST with some hint of westward propagation, particularly in the warm phase [cf. Neelin *et al.*, 1994]. The largest anomalies occur in a broad region in the eastern Pacific as observed, but the model warm events extend too far into the western Pacific, near  $160^{\circ}\text{E}$ ; similar behavior is seen in the hybrid coupled model of Barnett *et al.* [1993]. The observed warm phases shown in Figure 7b, however, rarely extend westward beyond the dateline. Consistent with observations, the model cold events have their strongest signature in the cold tongue region, with anomalies as large as  $-4^{\circ}\text{C}$ , as compared to the observations where negative anomalies rarely exceed  $-2^{\circ}\text{C}$ . Like the warm events, the model cold events also extend too far west, with a magnitude greater than  $-2.0^{\circ}\text{C}$  in the western central Pacific as compared with about  $-0.5^{\circ}\text{C}$  in the observations.

For the SVD-SW case (Figure 13b), several aspects of the simulation have changed. First, the westward extent of the warm events has been strongly curtailed. In this case, anomalous warming rarely extends west of the dateline. Second, the warming in the eastern Pacific has also been reduced by about  $0.5^{\circ}\text{C}$ . Third, the magnitude of the cold anomalies is reduced by about  $1^{\circ}\text{C}$  across the width of the basin. Fourth, the period of the oscillation has decreased, from 29 months in the Standard case to about 24 months in the SVD case. This latter difference is likely related to the

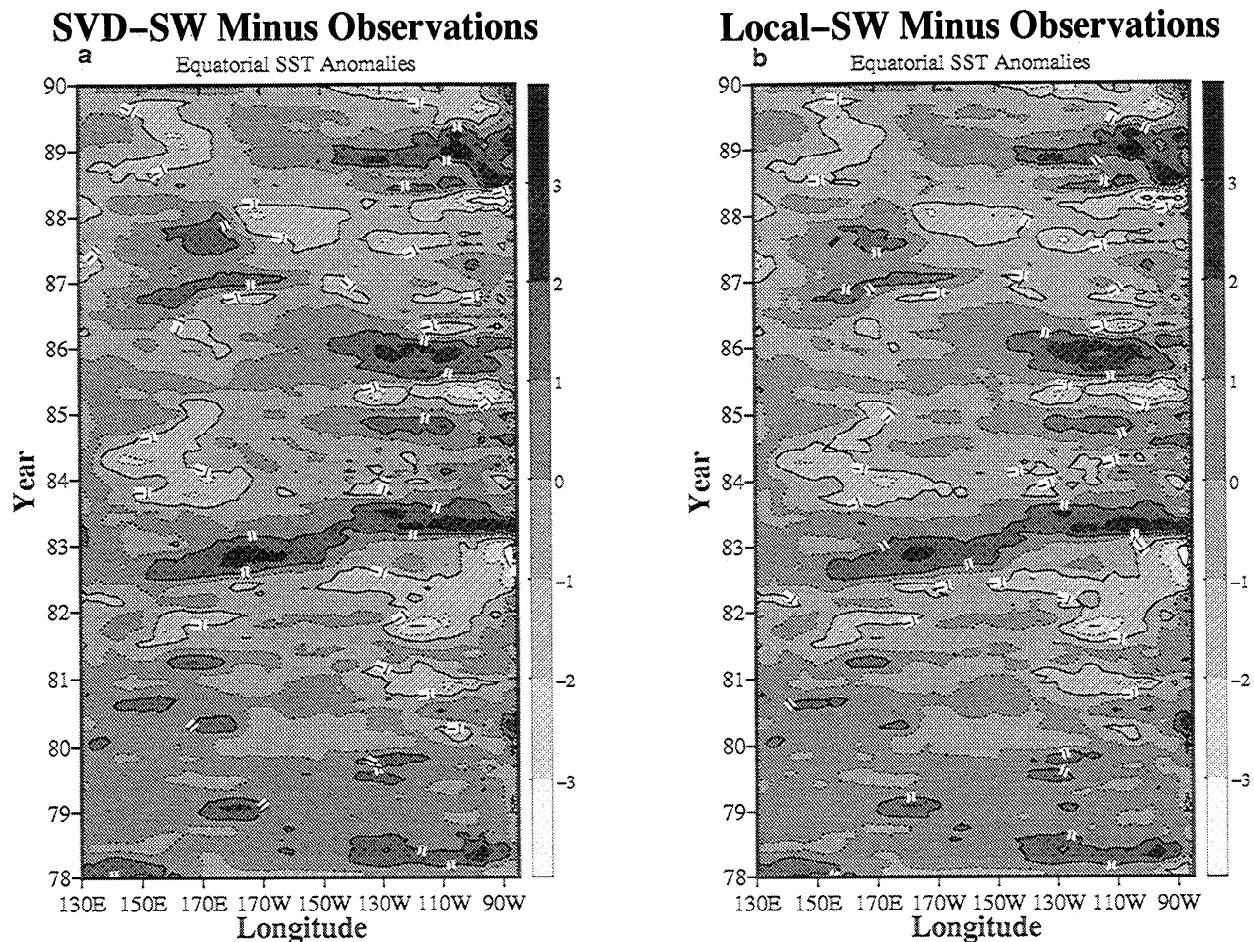


**Figure 8.** Same as Figure 7c, except for the (a) SVD-SW simulation and (b) local SW simulation.

diminished westward extent of the warm anomalies and the weaker amplitude of the oscillations, each of which would tend to decrease the period. With respect to the magnitude of the anomalies and their spatial characteristics, the inclusion of the SW feedback has resulted in better agreement between the simulated and observed interannual variability.

The simulation for the local SW case (Figure 13c) is very nearly identical to that of the SVD-SW case. This experi-

ment was designed to determine whether the implied (remote) covariability between SW in the central Pacific (i.e., Figure 1b) and SST in the eastern Pacific is important in establishing the character of the large-scale, low-frequency, negative feedback due to SST-forced cloudiness. The similar results between the SVD-SW and local SW simulations in this section (Figures 13b and 13c) and the previous section (Figures 8a and 8b) suggests that the large-scale, interannual, SST-forced component of the SW variability in the central Pacific may be accounted for by considering primarily the local SST anomaly.

### Time Series of SW-SST Mode

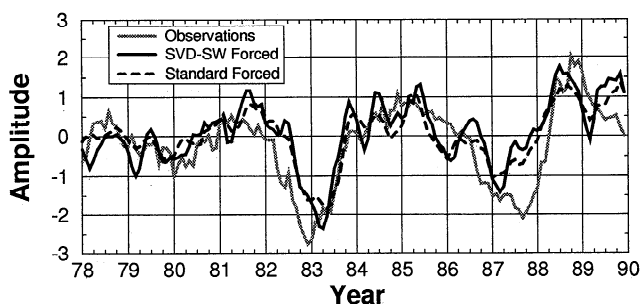


**Figure 9.** Projection of SST mode (Figure 1a) onto observed SST (thick gray line), SST from SVD-SW case (thick black line), and SST from Standard simulation (thick dashed line).

## 7. Summary and Discussion

In the simulations presented above we have attempted to assess the importance of the large-scale, low-frequency feedbacks associated with SST-forced cloudiness in the development and evolution of the ENSO phenomena. This feedback occurs because the equatorial warming associated with the El Niño phase of ENSO tends to produce anomalous atmospheric deep convection in the central Pacific, and thus a decrease of incoming SW at the surface. The diminished shortwave acts to cool the anomalously warm SST in the central Pacific and thus helps to limit the amplitude of the ENSO warm phase in this region. The reverse mechanism holds for the cold phase of ENSO, in which negative anomalies in convection/cloudiness occur in the central

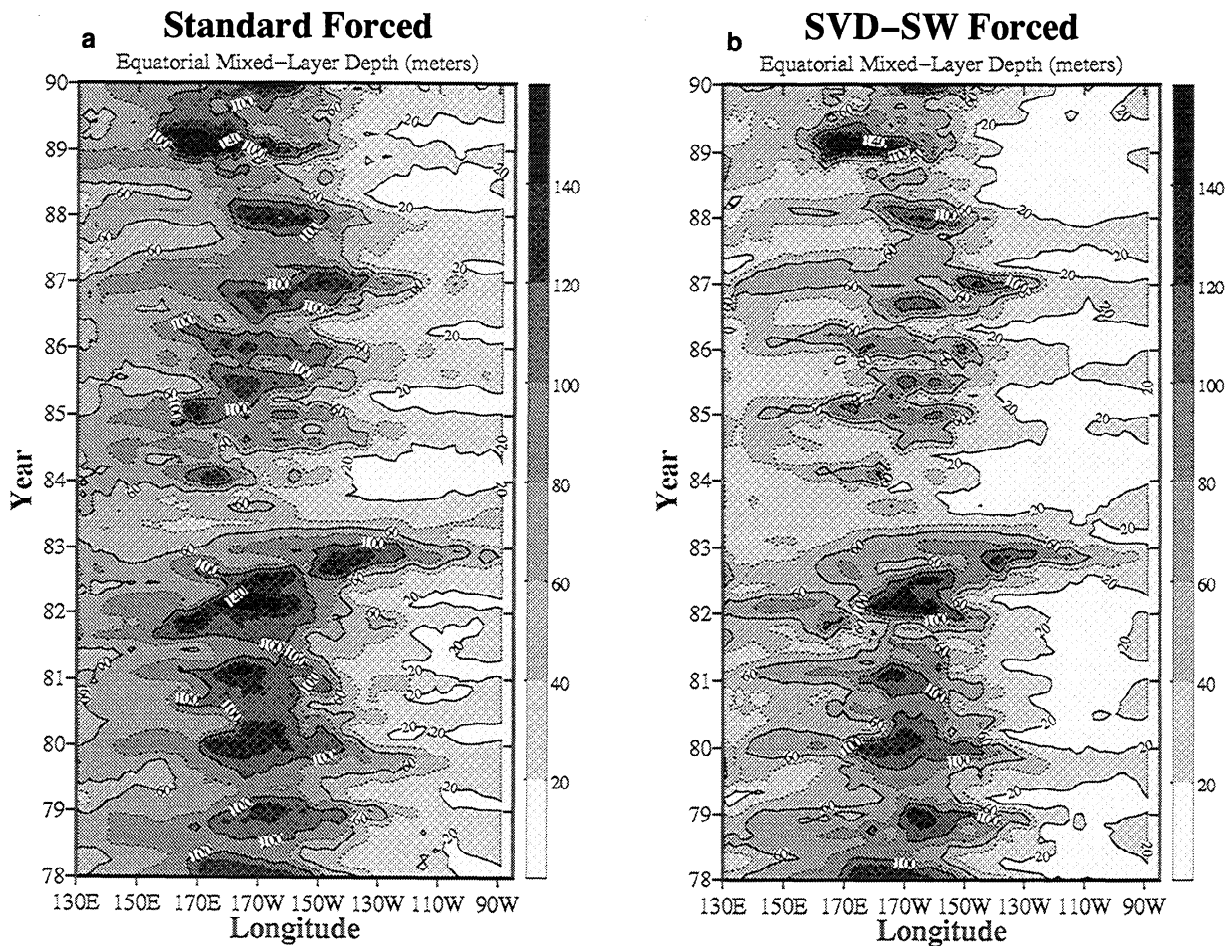


**Figure 10.** Time-longitude diagram of mixed-layer depth at the equator for the (a) Standard and (b) SVD-SW simulations. Mixed-layer values are given in meters and were computed as the depth where the subsurface temperature is 1°C less than the sea surface temperature. Equatorial sections are averaged between 0.5°N and 0.5°S.

Pacific due to the anomalously cool SST. This increases the downwelling surface shortwave and acts to warm the SST and thus reduce the magnitude of the cooling in the region.

Two shortwave feedbacks were developed to examine the effects on ENSO simulations using forced and hybrid-coupled ocean general circulation models. Each feedback scheme produced the largest shortwave response in the central Pacific near the dateline. For the SVD scheme the SW anomalies depended nonlocally on SST anomalies in the central and eastern Pacific, weighted as in Figure 1. For the local scheme the SW anomalies depended on the local SST anomaly weighted, as in Figure 6, with a spatially varying feedback amplitude.

The two feedback parameterizations were applied to the forced model, which in the standard configuration contains only seasonally varying SW. Both schemes behaved similarly but did not act entirely as expected, producing very modest changes to the simulated SST, and in some cases even increased SST slightly in the region of the applied negative feedback. A simplified box model analysis showed that when the SW feedbacks are applied in the forced configuration, there are secondary effects related to mixed-layer dynamics that come into play, which balance, and occasionally even outweigh, the surface heat flux damping

effect. This competing mechanism stems from a mean shallowing of the mixed layer by nonlinear interaction of mixing with the heat flux feedback. This shallowing induces an increased vertical temperature gradient and an enhanced response of the zonal velocity to the imposed winds, each of which acts to increase the magnitude of the SST anomalies near the dateline. In the cases of the SVD-SW and local SW cases, these two competing effects essentially balance, leaving the magnitude of the interannual SST anomalies essentially unchanged. Applying the observed SW anomalies (not coupled to the SST) produced changes in the simulated SST that were more consistent with expectations and with observations. For example, the  $40 \text{ W m}^{-2}$  SW reduction during the 1986–1987 warm event produced an  $0.8^\circ\text{C}$  cooling and the subsequent about a  $0.4^\circ\text{C}$  warming for about a  $20 \text{ W m}^{-2}$  SW increase in the subsequent La Niña period.

In the coupled simulations the feedback schemes produced modifications to the simulations which were more in line with what was expected. Both schemes reduced the westward extent of the anomalous warming from about  $150^\circ\text{E}$  in the standard configuration to  $160^\circ\text{W}$ , and they reduced the magnitude of the cold episodes across the Pacific by about  $1^\circ\text{C}$ . Finally, the period of the oscillations is reduced from about 29 months in the Standard configuration

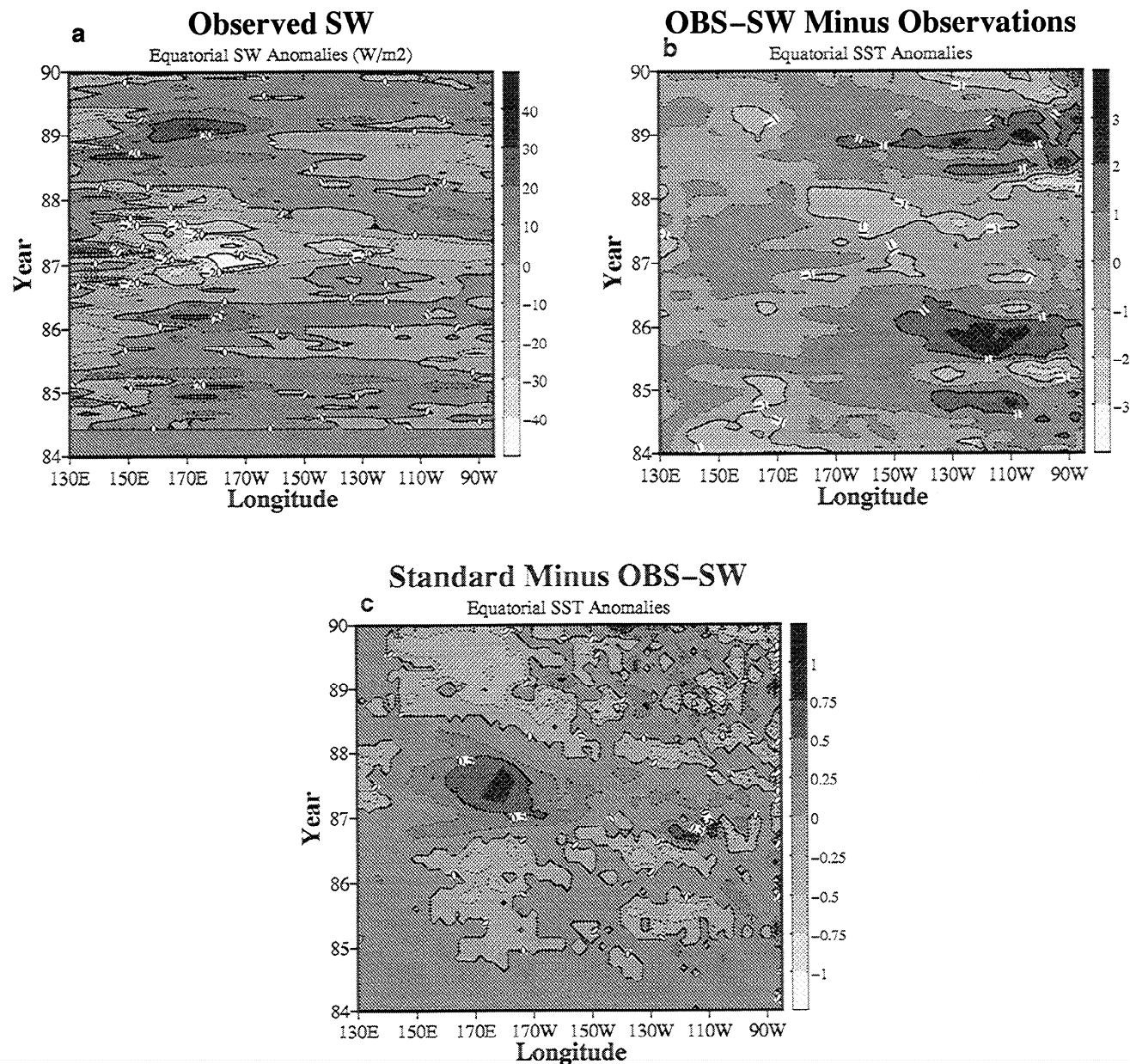


**Figure 11.** (a) Time-longitude diagram of the satellite-derived SW anomalies on the equator. (b) Same as Figure 7c, except for the simulation in which satellite-derived SW anomalies were applied. (c) Time-longitude diagram of the difference between the SST anomalies on the equator from Standard simulation and the simulation using observed SW anomalies. Equatorial sections are averaged between 1°N and 1°S.

to about 24 months in the cases with SW feedback. With the exception of the period decrease, the coupled model ENSOs with SW feedback tend to be in better agreement with observations.

The above results suggest that large-scale SW negative feedbacks tend to produce quantitative changes in the ENSO cycle but are not critical to the overall occurrence of the phenomena. This main conclusion could have been anticipated partly on the basis of scaling arguments: a negative feedback of  $20 \text{ W m}^{-2} \text{ K}^{-1}$  distributed over a 50-m depth gives a damping time scale of about 3 months; this may be roughly compared to ocean time scales affecting the mixed layer via dynamical processes; for instance, the process for upwelling subsurface anomalies into the mixed layer in the east central Pacific is of the order of 1 month. However,

because the SW feedbacks modify a nonlinear ENSO cycle, in a manner which is highly spatially dependent, and because appropriate scaling for coupled processes can be very different from that of uncoupled processes [e.g., Neelin, 1991], this result is more convincing, since it is obtained in a self-consistent model, with oceanic nonlinearities explicitly treated.

A secondary conclusion is that radiative feedbacks can interact significantly with wind stress feedbacks in the central Pacific region. This conclusion is motivated by the difference in the impacts of the SW feedback in the forced and coupled model experiments. This difference illustrates the importance of testing impacts of hypothesized processes in a coupled context, because when important parts of the system are specified—in this case the wind stress—the

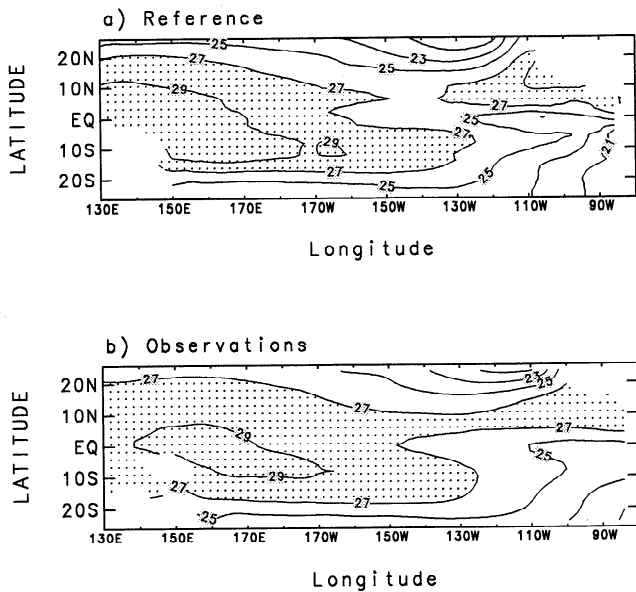


**Figure 12.** (a) Long-term mean SST from coupled model used as an initial and reference state. (b) Long-term mean SST from observations.

feedback can be significantly different. We also note that significant interaction of radiative feedbacks with mixing processes was found, although we place less emphasis on this.

Some caveats concerning these conclusions are nonetheless needed: the ocean GCM is known to be sensitive to the vertical mixing parameterization (for example, compare the coupled results to those of SNG (1994)); the simulation of the 1987–1988 ENSO warm phase attests to the model being less than perfect, and the present formulation of the surface boundary conditions do not allow for active evaporation–wind feedbacks to occur. It has been suggested that such feedbacks can be important in the maintenance and propagation of large-scale atmospheric convection in the tropics [Neelin *et al.*, 1987; Emanuel, 1987] and that they have been observed to play a significant role in the surface heat budget changes associated with ENSO [Liu and Gautier, 1990]. Since the evaporation–wind feedback can act as a positive feedback in association with ENSO changes (i.e., evaporation over the warm anomalies is often reduced due to diminished wind speeds and a decreased air–sea specific humidity difference), it is possible that SW feedbacks would become more important if this mechanism were better accounted for in the model formulation. Combining both these

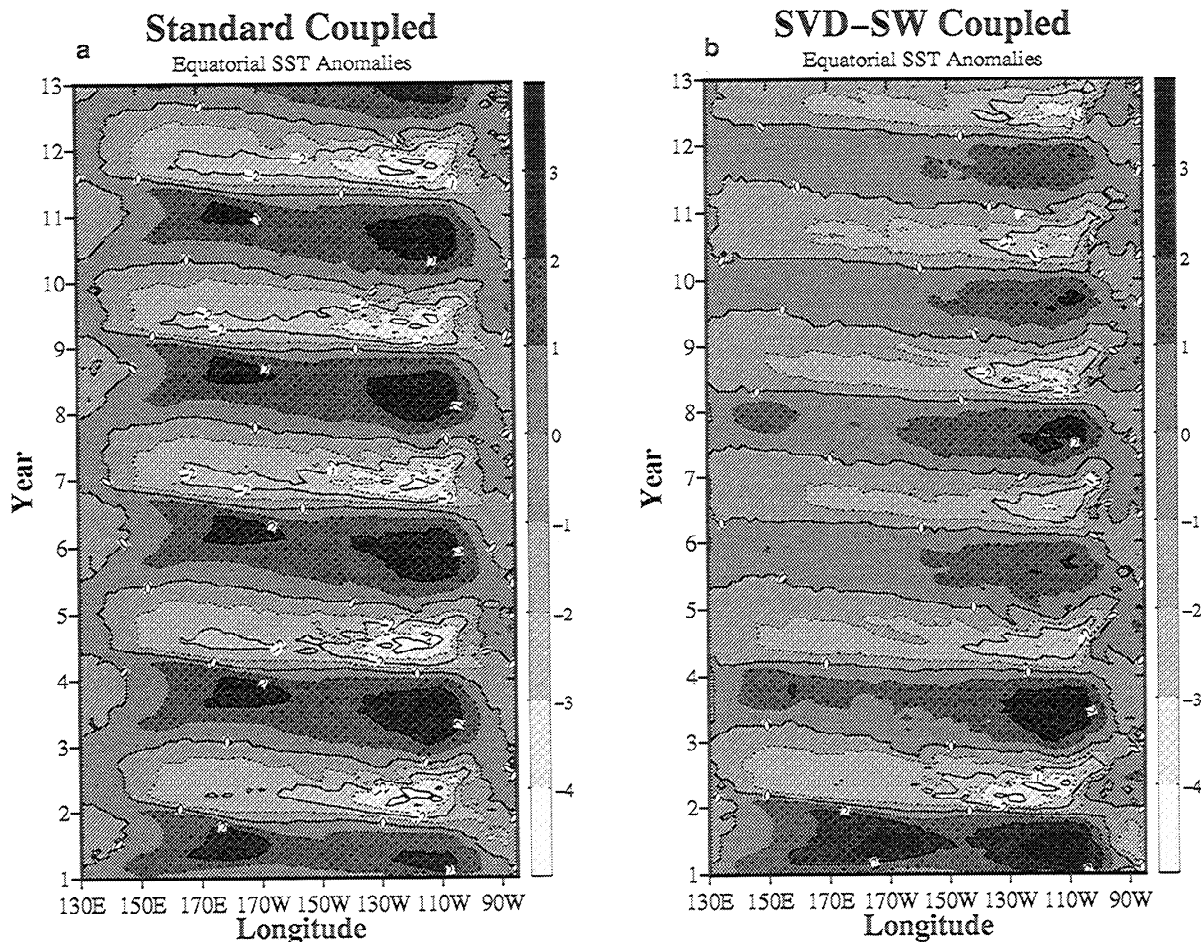


**Figure 13.** Time-longitude diagram of SST anomalies on the equator from the coupled model simulations using the (a) Standard, (b) SVD-SW feedback, and (c) Local-SW feedback configurations. Equatorial sections are averaged between 1°N and 1°S.

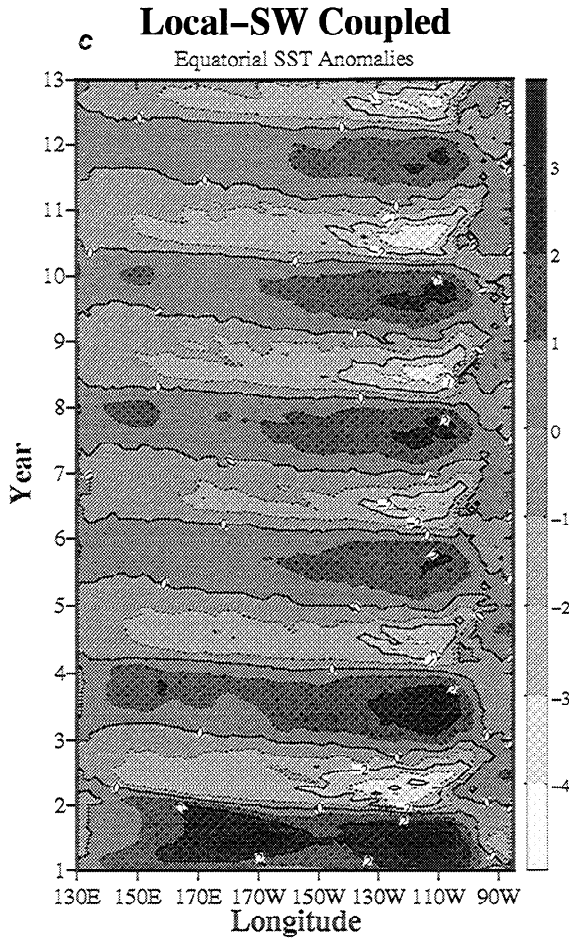


Figure 13. (continued)

feedbacks is an important next step and is an area currently being investigated.

The fact that the two SW feedback schemes tested have nearly the same impact suggests that SST changes in the eastern Pacific may not be important in the manifestation and subsequent impacts of the SW feedback in the central Pacific. This does not mean that SST anomalies in the eastern Pacific don't play a role in modifying the atmospheric circulation to enhance, or help initiate, convection in the central Pacific. The lack of difference between the local and nonlocal cases simply implies that the spatial correlation scale in the ocean dynamics affecting SST in the ENSO cycle is sufficiently large that nonlocal effects from the atmospheric side can be omitted or hidden in the spatial variation of the local feedback. (The atmospheric response is nonlocal in the wind response in this model in all coupled cases.) We also find that the effects of any time lag between the warming in the eastern Pacific (where it usually first appears) and the central Pacific (where convection usually develops) is not important to the overall evolution of the ENSO phenomena. This idea was tested through a time-lagged SVD analysis of SST and SW. This analysis showed that when the SST leads the SW by about 1 month, the percentage of covariability explained by the first modes increases by a few percent. When this time lag was taken into account in the coupled model SVD-SW simulation, i.e., SW this month is determined from SST last month, the results were qualitatively

the same as those shown in Figure 13b. Therefore these results indicate that it may be necessary to take into account only local SST variability when parameterizing ENSO-scale SW feedbacks in simulations of the tropical Pacific.

### Appendix: Box Model Analysis of SW Feedback in Forced Simulations

Figure 14 shows time series of several quantities taken from the Standard (solid) and SVD-SW (dashed) simulations for the region 177°E–177°W and 0.5°S–0.5°N—the region where the applied SW damping is greatest. Figure 14a shows the zonal wind stress forcing which is specified and is the same for both simulations. Figures 14b–14e show the SST anomalies, mixed-layer depth (defined as the depth where the ocean temperature differs from the surface by 1°C), and the zonal and vertical velocity anomalies averaged over the depth of the mixed layer, respectively. The high degree of similarity between the two SST time series can be understood by analyzing a simplified form of the local surface heat budget. In this region the evolution of the SST anomaly is largely governed by anomalous zonal advection of the mean zonal temperature gradient, anomalous vertical advection of the mean thermocline, and local thermodynamic damping processes. Given these assumptions, the temperature evolution can be expressed as

$$\frac{\partial T'}{\partial t} = -u' \frac{\partial \bar{T}}{\partial x} - w' \frac{\partial \bar{T}}{\partial z} - \frac{(\epsilon_q + \epsilon_s)}{\rho c_p H} T' \quad (\text{A1})$$

where  $\bar{T}$  and  $T'$  are the SST mean and anomaly values,  $u'$  and  $w'$  are the anomalous zonal and vertical velocities,  $\epsilon_q$  and  $\epsilon_s$  represent local damping processes primarily attributed to evaporation and shortwave feedbacks, respectively,  $H$  is the mean mixed-layer depth,  $\rho$  is the density, and  $c_p$  is the specific heat capacity. If we further assume that the anomalous zonal and vertical velocities are roughly proportional to the anomalous zonal wind stress (compare Figures 14a and 14d–14e),

$$u' = \alpha \tau'_x \quad (\text{A2})$$

$$w' = \beta \tau'_x$$

where  $\tau'_x$  is the zonal wind stress anomaly and  $\alpha$  and  $\beta$  are linear proportionality constants, then the equation can be rewritten as

$$\frac{\partial T'}{\partial t} = -\left( \alpha \frac{\partial \bar{T}}{\partial x} + \beta \frac{\partial \bar{T}}{\partial z} \right) \tau'_x - \frac{(\epsilon_q + \epsilon_s)}{\rho c_p H} T' \quad (\text{A3})$$

For a system forced with periodic wind stress variability of the form  $\tau'_x = A \cos(\omega t)$ , the oscillatory part of the solution has amplitude

$$\frac{GA}{(E^2 + \omega^2)^{1/2}} \quad (\text{A4})$$

where

$$E = \frac{(\epsilon_q + \epsilon_s)}{\rho c_p H}$$

and

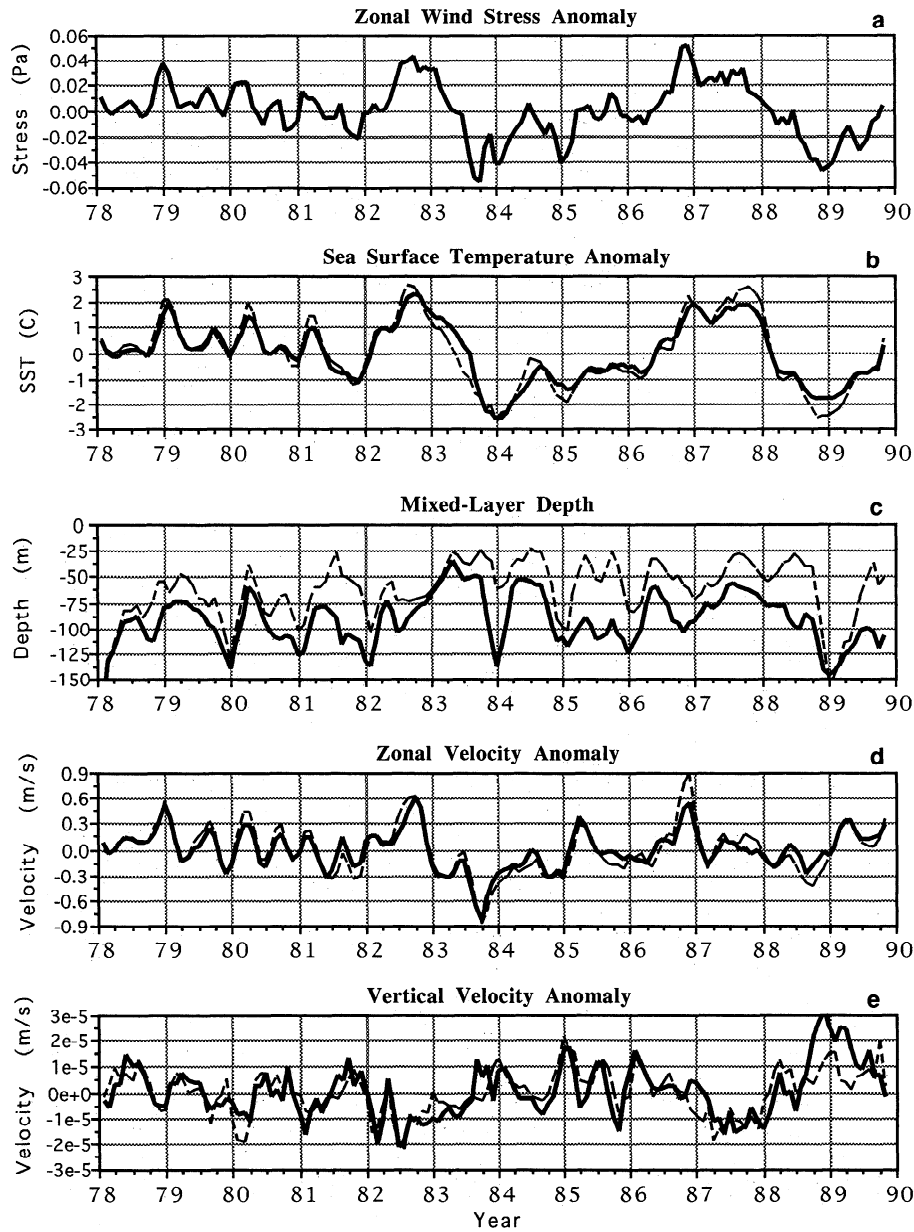


**Figure 14.** Time series of (a) specified zonal wind stress anomaly, (b) SST anomaly, (c) mixed-layer depth, (d) zonal velocity anomaly, and (e) vertical velocity anomaly from the Standard (solid) and SVD-SW (dashed) uncoupled simulations. The values are averages for the domain 177°E–177°W and 0.5°S–0.5°N. The mixed layer is defined as the depth where the ocean temperature differs from the surface by 1°C, and the zonal and vertical velocity anomalies averaged over the depth of the mixed layer.

$$G = -\left(\alpha \frac{\partial \bar{T}}{\partial x} + \beta \frac{\partial \bar{T}}{\partial z}\right)$$

Table 1 provides the representative values for the Standard and SVD-SW forced simulations needed to evaluate the SST anomaly amplitude (A4) for the box domain described above. In this table the value of the mean zonal gradient computed over the length of the “box,” the mixed-layer depth ( $H$ ) is the corresponding series’ mean of Figure 14c, the vertical gradient was computed by time-averaging the quantity  $(1^\circ/H)$ , the values of  $u'$ ,  $w'$ , and  $\tau'_x$  in Figures 14a, 14d, and 14e were used to obtain  $\alpha$  and  $\beta$ , and  $\varepsilon_q$  is the value of the negative feedback discussed in section 4.

The resulting amplitudes given by the box model using input values from both the Standard and SVD-SW simulations give a result of 2.7°K in each case. This magnitude is consistent with the numerical simulations (Figure 14b), indicating that the simple box model does indeed capture the most important elements of the surface heat budget. Closer inspection of the parameter values given in Table 1 reveals how changes primarily in  $H$ ,  $\partial \bar{T} / \partial z$ , and  $\alpha$  induced by the applied SW feedback lead to compensating effects in the  $E$  and  $G$  terms of the amplitude expression (A4). First, the mixed layer ( $H$ ) is shallower due to the nonlinear effects of the added SW feedback. During periods when the SST is low, there is a positive surface heat flux anomaly due to the

**Table 1.** Parameter Values for the Box-Model Heat Budget Analysis

Parameter	Standard	SVD-SW
$\partial\bar{T}/\partial x$ , K m <sup>-1</sup>	$-7.6 \times 10^{-7}$	$-7.4 \times 10^{-7}$
$\partial\bar{T}/\partial z$ , K m <sup>-1</sup>	$1.2 \times 10^{-2}$	$2.1 \times 10^{-2}$
$\alpha$ , m s <sup>-1</sup> Pa <sup>-1*</sup>	5.4 (0.6)	8.3 (0.7)
$\beta$ , m s <sup>-1</sup> Pa <sup>-1*</sup>	$-3.1 \times 10^{-4}$ (-0.7)	$-2.8 \times 10^{-4}$ (-0.6)
$\varepsilon_q$ , W m <sup>-2</sup> K <sup>-1</sup>	20	20
$\varepsilon_s$ , W m <sup>-2</sup> K <sup>-1</sup>	0	20
$H$ , m	85	65
$E$ , s <sup>-1</sup>	$5.9 \times 10^{-8}$	$1.5 \times 10^{-7}$
$G$ , K s <sup>-1</sup> Pa <sup>-1</sup>	$7.8 \times 10^{-6}$	$1.2 \times 10^{-5}$
$\omega$ , s <sup>-1</sup>	$1.0 \times 10^{-7}$	$1.0 \times 10^{-7}$
$A$ , Pa	0.04	0.04
$GA/(E^2 + \omega^2)^{1/2}$ , K	2.7	2.7

Numbers in parentheses are linear correlation values (see (A2)).

SW feedback which enhances the stratification within the surface layers and thus tends to reduce the mixed-layer depth. During periods when the SST is high there is a negative surface heat flux anomaly, which has to work against strong stratification at the base of the mixed layer in order to increase the mixed-layer depth. Thus even though the mean value of the heat flux added from the SW feedback is near zero over the course of the simulation, its mean effects on the mixed layer are not zero and correspond to a mean shallowing of about 20 m. Second, because the mixed layer is shallower in the SVD-SW simulation, the mean vertical temperature gradient ( $\partial\bar{T}/\partial z$ ) is increased. This in turn induces less mixing and more vertical shear, both of which lead to a zonal circulation more tightly concentrated in the upper layers (i.e., enhanced  $\alpha$ ) and thus more responsive to the specified wind stress anomalies.

In summary, the added SW feedback in the forced SVD-SW case not only increases the local negative feedback on SST (i.e.,  $\varepsilon_s > 0$ ) but also induces a mean shallowing of the mixed layer, each of which results leads to a decrease in the amplitude of the SST anomaly through their effects on  $E$ . Compensating this effect are a larger mean vertical temperature gradient and a stronger zonal velocity response for a given wind stress (i.e.,  $\alpha$ ), each of which leads to an increase in the SST anomaly amplitude through their effects on  $G$ . In the cases of the wind-forced simulations represented here, the effects of increased  $G$  and  $E$  tend to balance such that the SST anomaly amplitude is the same for the Standard and SW-SVD cases.

**Acknowledgments.** Support for this study has been provided by the National Oceanic and Atmospheric Administration (NOAA) Postdoctoral Program in Climate and Global Change (D.W.), NOAA NA46GP0244/NA26GP0114 (B.B., D.N.) and NA16RC0524 (C.G.), Centre National de la Recherche Scientifique (B.B.), National Science Foundation (NSF) ATM-9215090 (D.N.), and the National Aeronautics and Space Administration JPL959177 (C.G.). The authors thank Hsin-Hsin Syu for providing the original version of the HCM code, David Gutzler for providing the model atmosphere used in the coupled simulations and Nicholas Graham for helpful discussion regarding CCA. Supercomputing support was provided by Florida State University and the NSF supported National Center for Atmospheric Research and San Diego Supercomputing Center. Computation equipment and software for this research was provided by Digital Equipment Corporation under research project Sequoia 2000. Graphics support was provided by the National Center for Supercomputing Applications, Richard Ma, and Kenny Toh.

## References

- Barnett, T. P., M. Latif, N. E. Graham, M. Flugel, S. Pazan, and W. White, ENSO and ENSO-related predictability, I, Prediction of equatorial Pacific sea surface temperature with a hybrid coupled ocean-atmosphere model, *J. Clim.*, **6**, 1545–1566, 1993.
- Battisti, D. S., The dynamics and thermodynamics of a warming event in a coupled tropical atmosphere/ocean model, *J. Atmos. Sci.*, **45**, 2889–2919, 1988.
- Blanke, B., and P. Delecluse, Variability of the tropical Atlantic Ocean simulated by a general circulation model with two different mixed layer physics, *J. Phys. Oceanogr.*, **23**, 1363–1388, 1993.
- Bretherton, C. S., C. Smith, and J. M. Wallace, An intercomparison of methods for finding coupled patterns in climate data, *J. Clim.*, **5**, 541–560, 1992.
- Cane, M. A., Oceanographic events during El Niño, *Science*, **222**, 1189–1195, 1983.
- Chertock, B., R. Frouin, and R. C. J. Somerville, Global monitoring of net solar irradiance at the ocean surface: Climatological variability and the 1982–83 El Niño, *J. Clim.*, **4**, 639–650, 1991.
- Cox, M. D., A primitive equation, 3-dimensional model of the ocean, *GFDL Ocean Group Tech. Rep. 1*, Geophys. Fluid Dyn. Lab./Natl. Ocean. Atmos. Admin., Princeton, N. J., 1984.
- Emanuel, K. A., An air-sea interaction model of intraseasonal oscillations in the tropics, *J. Atmos. Sci.*, **44**, 2324–2340, 1987.
- Gadgil, S., P. V. Joseph, and N. V. Joshi, Ocean-atmosphere coupling over monsoon regions, *Nature*, **312**, 141–143, 1984.
- Garcia, O., Atlas of Highly Reflective Clouds for the Global Tropics: 1971–1983, Environ. Res. Lab., Natl. Ocean. and Atmos. Admin., U.S. Dep. of Commer., Boulder, Colo., 1985.
- Gautier, C., G. Diak, and S. Masse, A simple physical model to estimate incident solar radiation at the surface from GOES satellite data, *J. Clim. Appl. Meteorol.*, **23**, 1380–1386, 1980.
- Gent, P. R., and J. J. Tribbia, Simulation and predictability in a coupled TOGA model, *J. Clim.*, **6**, 1843, 1993.
- Giese, B. S., and D. R. Cayan, Surface heat flux parameterizations and tropical Pacific SST simulations, *J. Geophys. Res.*, **98**, 6979–6989, 1993.
- Graham, N. E., and T. P. Barnett, Sea surface temperature, surface wind divergence, and convection over tropical oceans, *Science*, **238**, 657–659, 1987.
- Graham, N. E., J. Michaelson, and T. P. Barnett, An investigation of the El Niño–Southern Oscillation cycle with statistical models, 1, Predictor field characteristics, *J. Geophys. Res.*, **92**, 14,251–14,270, 1987.
- Gruber, A., and A. F. Krueger, The status of the NOAA outgoing longwave radiation data set, *Bull. Am. Meteorol. Soc.*, **65**, 958–962, 1984.
- Harrison, D. E., Equatorial sea surface temperature sensitivity to net surface heat flux: Some ocean circulation model results, *J. Clim.*, **4**, 539–549, 1991.
- Horel, J., and A. G. Cornejo-Garrido, Convection along the coast of northern Peru during 1986: Spatial and temporal variation of clouds and rainfall, *Mon. Weather Rev.*, **114**, 2091–2105, 1986.
- Hurlburt, H. E., J. C. Kindle, and J. J. O'Brien, A numerical simulation of the onset of El Niño, *J. Phys. Oceanogr.*, **6**, 621–631, 1976.
- Lau, N.-C., Modelling the seasonal dependence of the atmospheric response to observed El Niños in 1962–76, *Mon. Weather Rev.*, **113**, 1970–1996, 1985.
- Legler, D. M., and J. J. O'Brien, Atlas of Tropical Pacific Wind Stress Climatology 1971–1980, Dep. of Meteorol., Fla. State Univ., Tallahassee, 1984.
- Levitus, S., Climatological atlas of the world ocean, *NOAA Prof. Pap. 13*, U.S. Govt. Printing Office, Washington, D. C., 1982.
- Liebmann, B., and D. L. Hartmann, Interannual variations of outgoing IR associated with tropical circulation changes during 1974–1978, *J. Atmos. Sci.*, **39**, 1153–1162, 1982.
- Liu, W. T., and C. Gautier, Thermal forcing on the tropical Pacific from satellite data, *J. Geophys. Res.*, **95**, 13,209–13,217, 1990.
- McCreary, J., Eastern tropical response to changing wind systems with application to El Niño, *J. Phys. Oceanogr.*, **6**, 632–645, 1976.
- Neelin, J. D., A hybrid coupled general circulation model for El Niño studies, *J. Atmos. Sci.*, **47**, 674–693, 1990.
- Neelin, J. D., The slow sea surface temperature mode and the fast-wave limit: Analytic theory for tropical interannual oscillations, *J. Atmos. Sci.*, **47**, 694–719, 1990.

- tions and experiments in a hybrid coupled model, *J. Atmos. Sci.*, **48**, 584–606, 1991.
- Neelin, J. D., and I. M. Held, Modeling tropical convergence based on the moist static energy budget, *Mon. Weather Rev.*, **115**, 3–12, 1987.
- Neelin, J. D., I. M. Held, and K. H. Cook, Evaporation-wind feedback and low frequency variability in the tropical atmosphere, *J. Atmos. Sci.*, **44**, 2341–2346, 1987.
- Neelin, J. D., M. Latif, and F. F. Jin, Dynamics of coupled ocean-atmosphere models: The tropical problem, *Annu. Rev. Fluid Mech.*, **26**, 617–659, 1994.
- Oberhuber, J. M., An atlas based on the COADS data set, *Rep. 15*, Max-Planck-Institut für Meteorologie, Hamburg, Germany, 1988.
- Paulson, C. A., and J. J. Simpson, Irradiance measurements in the upper ocean, *J. Phys. Oceanogr.*, **7**, 952–956, 1977.
- Peters, H., M. C. Gregg, and J. M. Toole, On the parameterization of equatorial turbulence, *J. Geophys. Res.*, **93**, 1199–1218, 1988.
- Philander, S. G. H., The response of equatorial oceans to a relaxation of the trade winds, *J. Phys. Oceanogr.*, **11**, 176–189, 1981.
- Philander, S. G. H., and A. Seigel, Simulation of El Nino of 1982–83, in *Coupled Ocean-Atmosphere Models*, edited by J. C. J. Nihoul, pp. 517–541, Elsevier, New York, 1985.
- Philander, S. G. H., R. C. Pacanowski, N. C. Lau, and M. J. Nath, Simulation of ENSO with a global atmospheric GCM coupled to a high-resolution, tropical Pacific ocean GCM, *J. Clim.*, **5**, 308–329, 1992.
- Ramanathan, V., and W. Collins, Thermodynamic regulation of ocean warming by cirrus clouds deduced from observations of the 1987 El Nino, *Nature*, **351**, 27–32, 1991.
- Rasmusson, E. M., and J. M. Wallace, Meteorological aspects of the El Nino/southern oscillation, *Science*, **222**, 1195–1202, 1983.
- Reynolds, R. W., A real-time global sea surface temperature analysis, *J. Clim.*, **1**, 75–86, 1988.
- Rosati, A., and K. Miyakoda, A general circulation model for upper ocean simulation, *J. Phys. Oceanogr.*, **18**, 1601–1626, 1988.
- Rossow, W. B., and R. A. Schiffer, ISCCP cloud data products, *Bull. Am. Meteorol. Soc.*, **72**, 2–20, 1991.
- Seager, R., S. E. Zebiak, and M. A. Cane, A model of the tropical Pacific sea surface temperature climatology, *J. Geophys. Res.*, **93**, 1265–1280, 1988.
- Simpson, J. J., and C. A. Paulson, Mid-ocean observations of atmosphere radiation, *Q. J. R. Meteorol. Soc.*, **105**, 487–502, 1979.
- Syu, H.-H., J. D. Neelin, W. Weibel, and D. Gutzler, Tropical ocean-atmosphere interaction with a hybrid coupled GCM: Seasonal cycle and interannual variability, paper presented at Fourth Symposium on Global Change Studies, Am. Meteorol. Soc., Anaheim, Calif., Jan. 18–21, 1993.
- Waliser, D. E., and N. E. Graham, Convective cloud systems and warm-pool SSTs: Coupled interactions and self-regulation, *J. Geophys. Res.*, **98**, 12,881–12,893, 1993.
- Waliser, D. E., N. E. Graham, and C. Gautier, Comparison of the highly reflective cloud and outgoing longwave data sets for use in estimating tropical deep convection, *J. Clim.*, **6**, 331–353, 1993.
- Wang, T., Satellite-derived long term net solar radiation over the global ocean surface: Its relationship to low frequency SST variation and El Nino, Master's thesis, Univ. of Calif., Santa Barbara, 1994.
- Zebiak, S. E., and M. A. Cane, A model El Nino southern oscillation, *Mon. Weather Rev.*, **115**, 2262–2278, 1987.
- B. Blanke, Laboratoire d'Océanographie Dynamique et de Climatologie, Université Pierre et Marie Curie-Case 100, 4, place Jussieu, 75252, Paris Cedex 05, France. (e-mail: bbl.@lodyc.jussieu.fr)
- C. Gautier, Earth Space Research Group, University of California at Santa Barbara, Santa Barbara, CA 93106. (e-mail: gautier@crseo.ucsb.edu)
- J. D. Neelin (corresponding author), Department of Atmospheric Sciences, University of California, Los Angeles, CA 90024. (e-mail: neelin@atmos.ucla.edu)
- D. E. Waliser, Institute for Terrestrial and Planetary Atmospheres, State University of New York, Stony Brook, NY 11794. (e-mail: waliser@terra.msfc.sunysb.edu)

(Received February 28, 1994; revised July 13, 1994; accepted September 1, 1994.)